DEVELOPMENT AND ANALYSIS OF IMPROVED THERMOELECTRIC MATERIALS

An Undergraduate Honors Thesis

Submitted to the Department of Mechanical Engineering

The Ohio State University

In Partial Fulfillment of the Requirements

For Graduation with Distinction in Mechanical Engineering

Luyang Wang

November, 2018

ABSTRACT

Thermoelectric cooling devices, also called Peltier coolers, are devices based on the thermoelectric effect of materials and act in cooling mode. By adding an electrical potential on two sides of the material, a temperature gradient will be created. Thermoelectric cooling devices have many advantages, when compared to the commonly used compression-used refrigerators. For example, refrigerant-free, vibration free and compact. However, a vital disadvantage of thermoelectric cooling device is that it has a much lower device efficiency, comparing to compressor-based refrigerators. Thermoelectric coolers offer around 10-15% efficiency of ideal Carnot cycle, while compressor-based refrigerators provide 40-60% efficiency ideal Carnot cycle. The efficiency of thermoelectric cooler is influenced by the performance of thermoelectric used. Therefore, the purpose of this project was to improve the thermoelectric performance of Bi-Sb alloy. Bi-Sb alloys are of interest for thermoelectric cooling devices and it is believed that their heat pump efficiency can be enhanced by using CuBr resonant impurities. This project involves the synthesis of polycrystalline Bi-Sb alloys with different amounts of CuBr prepared via ingot casting. A concentrated master sample, with 0.5% CuBr, was developed first. Then, 2 times, 5 times and 10 times diluted samples was developed by diluting the master sample. After measurement, the master sample was found to have best thermoelectric performance, with a ZT of 0.27. The second step was to develop a single-crystalline sample via zone melting with the master sample mentioned above. The single-crystalline sample was found to have huge enhancement in thermoelectric performance, the ZT value of it was found to be 0.41. The results prove that CuBr dopant does enhanced the heat pump efficiency of Bi-Sb alloy. However, it is not as much as expected. Further effort can be done to improve the efficiency even more.

ACKNOWLEDGEMENTS

First of all, I would like to thank my advisor, Prof. Joseph P. Heremans. Without him, I wouldn't be able to start this project or even think about doing this. He was always willing to guide me when I was confused. He led me into the world of scientific research, which sometimes can be frustrating but mostly engaging and fascinating.

I would like to thank Dr. Koen Vandaele for his help and advice during the whole process of this project. He has been a great mentor who not only trained me how to mount samples and adjusted measurement devices, but also explained all the difficult concepts to me patiently. I couldn't have done this without his generous help.

I would also like to thank Bin He and Yuanhua Zheng for helping me find all kinds of materials to read, and explaining all those elusive concepts in solid physics. With their help I have a better scope of thermoelectric materials and the physical meaning behind this project.

Table of Contents

Table of Figures

Chapter 1: Introduction

1.1 Focus of Thesis

The most commonly used cooling device in our daily life are mechanical compressors based on thermodynamic cycles. However, there are some noticeable disadvantages for mechanical compressors. First, the compressor itself occupies a lot of space and is normally very heavy. Second, it causes vibrations and noise while working. Third, the refrigerant used is normally toxic, flammable, and environmentally harmful. On the other hand, thermoelectric cooling devices, also called Peltier coolers, provide a solution to the aforementioned issues encountered in compression-based refrigerators. Namely, they are solid-state devices, which do not require cooling liquids and do not have any moving parts. They operate vibration free, have a long lifetime, and are and compact.

Thermoelectric devices are based on the thermoelectric effect and can act in power generation or cooling mode. A temperature gradient in the material creates an electrical potential between the hot and cold side, and an electrical potential creates a temperature gradient [1]. The thermoelectric effects arise because charge carriers in metal and semiconductors are free to move much, while carrying both charger and heat [2]. Because we can start from either the temperature gradient or the electrical potential, here, I have chosen to focus on using electrical potential to create a temperature gradient in this project, which means mainly efforts was devoted into synthesizing and analyzing thermoelectric materials used for thermoelectric cooler.

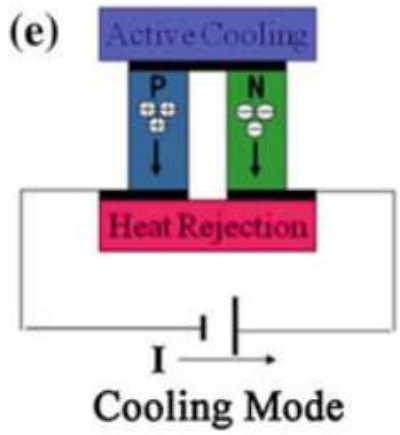

Figure 1: Thermoelectric couple for cooler [1]

The basic ideal of a thermoelectric cooler is shown in Figure 1. Two semi-conductors, one p-type and one n-type, are connected in series. P-type semi-conductors contain free holes (positive charge carriers), and n-type semiconductors contain free electrons (negative charge carriers). When they are connected as shown in figure 1, the electrical potential will drive both of them moving from top to bottom. As stated before, those carriers not only carry charge but also heat. So, when the holes and electrons go from top to bottom, heat will also be transported from top to bottom, which will create a cold side on top side relative to the hot side on bottom. In real applications, as shown in Figure 2, thermoelectric devices always contain many thermoelectric couples like this. Normally, a heat sink is required to dissipate heat from the hot side.

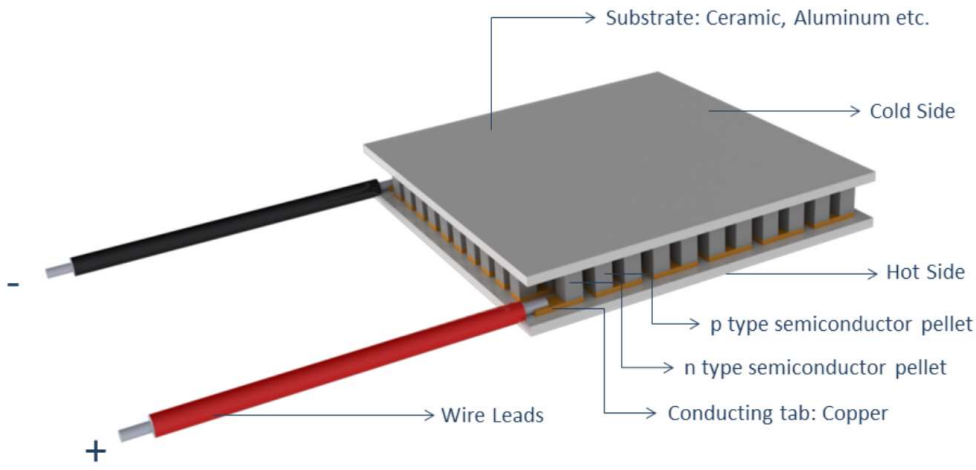

Figure 2: Actual Thermoelectric Cooler [3]

Despite the many advantages of thermoelectric coolers, a crucial disadvantage is their much lower efficiency as compared to coolers based on mechanical compressors [4]. The efficiency of current available thermoelectric cooling devices is only between 10-15% of Carnot efficiency, while that number for vapor compressors can reach about 60% [5]. The performance of thermoelectric material is quantified by the dimensionless thermoelectric material figure of merit, *ZT*:

$$ZT = \frac{\alpha^2 \sigma T}{\kappa}, \qquad (1)$$

with α (μV/K) the thermopower or Seebeck coefficient, σ the electrical conductivity (1/ Ωm,) κ (W/mK) thermal conductivity, and T (K) the absolute temperature, where the product of Seebeck square and electrical resistivity is defined as power factor. Consequently, the energy conversion efficiency for a thermoelectric cooler (η_{max}), can be written as:

$$\eta_{max} = \frac{T_c}{T_h - T_c} \frac{\sqrt{1+Z\bar{T}} - T_c/T_h}{\sqrt{1+Z\bar{T}}+1}, \quad (2)$$

with $\bar{T} = (T_h + T_c)/2$. In the equation for η_{max}, the first term is the Carnot efficiency. With the value of $Z\bar{T}$ increasing, the second term will go to 1 and the efficiency will go to Carnot efficiency. Thus, a higher *ZT* value will lead to a higher thermoelectric cooler efficiency. In that case, improving the performance of thermoelectric materials is essential for optimizing Peltier coolers.

To increase the value of *ZT*, a larger thermopower (absolute value of Seebeck coefficient), higher electrical conductivity and lower thermal conductivity are preferred. However, all of these characteristics are interrelated, which makes it's difficult to optimize all of them at the same time. First of all, the Seebeck coefficient is defined as as:

$$\alpha = \frac{8\pi^2 k_B^2}{3eh^2} m^* T \left(\frac{\pi}{3n}\right)^{2/3}, \quad (3)$$

where n is the carrier concentration, m^* is the effective mass of the carrier, h is the Planck constant and k_B is the Boltzmann constant. As shown in equation (3), with a lower carrier concertation there will be a larger Seebeck coefficient. However, a lower carrier concertation will result in a lower electrical conductivity. Because the electrical conductivity is given by:

$$\frac{1}{\rho} = \sigma = ne\mu, \quad (4)$$

where ρ is electrical resistivity, σ is electrical conductivity and μ is the carrier mobility. On the other hand, a higher effective mass will also increase the Seebeck coefficient. However, heavy carriers will move relatively slower, and means smaller mobilities. A smaller mobility will then result in a smaller electrical conductivity. The interrelationship between Seebeck coefficient and electrical conductivity makes it impossible to optimize those two at the same time.

What's more, another difficulty to increase zT comes from thermal conductivity, which is defined by equation (5a). As shown in equation (5a), thermal conductivity derives from two parts: electronic thermal conductivity (κ_e) and lattice thermal conductivity (κ_l). Electronic thermal conductivity comes from carriers that can transporting heat and is defined by equation (5b), while lattice thermal conductivity comes from phonons travelling through the lattice and is often calculated as the difference between κ and κ_e.

$$\kappa = \kappa_e + \kappa_l, \tag{5a}$$

$$\kappa_e = L\sigma T = ne\mu LT, \tag{5b}$$

where L is the Lorenz factor whose value can vary with carrier concentration [2]. In order to obtain a high zT value, thermal conductivity is desired to be low. With a smaller carrier concertation, the electronic thermal conductivity will be smaller. However, the electrical conductivity will also be smaller in that condition, which makes an inherent conflict. Furthermore, glasses normally have the smallest lattice thermal conductivity, but their mobility and effective mass are lower.

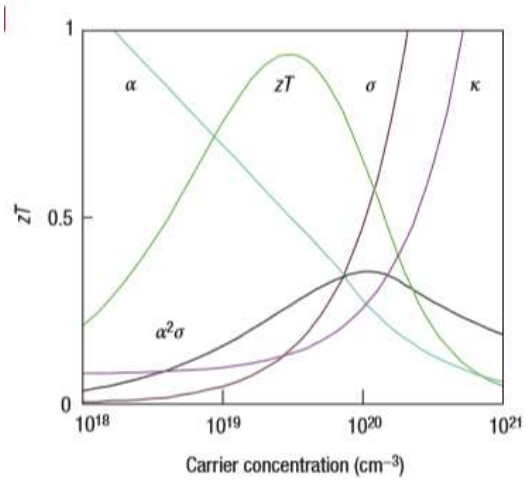

Figure 3: Relationship between α, σ, κ, Power Factor, zT and Carrier Concentration [2]

As shown in figure 3, Seebeck coefficient, thermal conductivity, electrical conductivity can not be optimized together. There has to be compromise to reach the highest zT. The peak of zT typically occurs at carrier concentrations between 10^{19} and 10^{21} carriers per cm^3, which is usually found in heavily doped semiconductors [2].

Solid materials are classified into 4 sections according to positions of their conduction and valence bands. The four sections are: metal, semimetal, semiconductor and insulator, as shown in Figure 4. The valance band is occupied by the outermost electrons who are still attached to the original atoms. The conduction band is occupied by free electrons who can move around to transfer heat and charge. In metals the conduction bands are partially filled, so there are many free electrons in metals, which results in the high electrical and thermal conductivity. In semimetals there are small overlaps between the bottom of the conduction band and the top of the valance band. Due to the small overlaps, semimetals have charge carriers of both types (holes and electrons), but only in a small amount. In semiconductors and insulators, there is a gap between the valence and conduction bands. The energy gap represents energy needed to transfer an electron from valence band to conduction band (Figure 5). In semiconductors the band gaps are relatively smaller than those in insulators. So, in semiconductors after a certain kind of excitation, for example heating, electrons on the top of valance bands will absorb enough energy and move to the bottom of conduction bands. In insulators, the gaps are too big for electrons to be excited, and have no free electrons to conduct electricity.

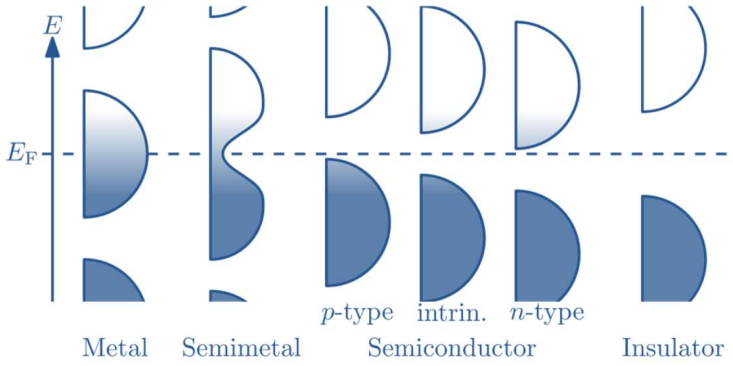

Figure 4: Images of Band Gap in Solids [3]

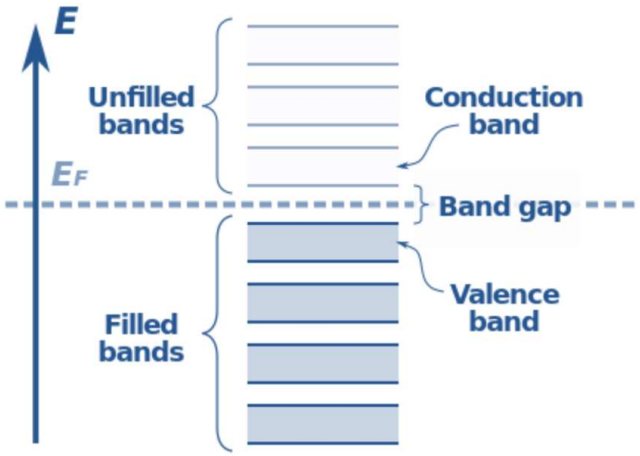

Figure 5: Image of Band Gap [3]

Semiconductors are mainly classified in to two kinds: intrinsic and extrinsic semiconductors. An intrinsic semiconductor is normally pure with same numbers of electrons and holes, which leads to a poor conductivity. An extrinsic semiconductor is an intrinsic semiconductor with a small amount of impurities. The process of adding impurities to an intrinsic semiconductor is called doping process, and this process will improve the conductivity of the intrinsic semiconductor. The impurities added can make semiconductors either negative charge conductor (n-type) or positive charge conductor (p-type), as shown in Figure 6.

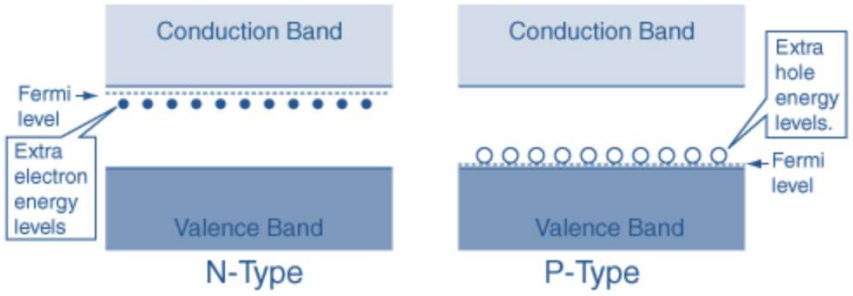

Figure 6: N-type and P-type semiconductors [3]

1.2 Significance of Research

For several decades, the *zT* value for commercial material has been limited to about 1 in all temperature ranges [6]. Consequently, the low *zT* value restrains the development of thermoelectric cooling devices as their performance is inferior to conventional cooling systems. Thus, the development of new materials with higher *zT* values has attracted significant scientific interest. There are two major approaches to improve the *zT* value of a thermoelectric material: decrease the lattice thermal conductivity using phonon scattering and increase the power factor. Recent *zT* advances include work from Heremans and coworkers. In 2008, they succeeded in increasing the *zT* of p-type PbTe to above 1.5 at 773 K by adding thallium impurity levels to enhance the Seebeck coefficient [6], which is also the mechanism used in this thesis. In 2012, Biswas et al. enhanced the thermoelectric performance of PbTe to zT= 2.2 at 915 K. by adding SrTe at a concentration of 4 mole percent to decrease the lattice thermal conductivity [7].

Although, the thermoelectric performance of PbTe alloys are excellent, the high price of tellurium and the restricted use of lead makes impractical for wide use. On the other hand, a nontoxic and inexpensive thermoelectric material is $Bi_{1-x}Sb_x$. However, its *zT* is quite low; it

reaches about 0.4 to 0.6. In 1964, researches at the Battelle Memorial Institute reported that $Bi_{88}Sb_{12}$ alloy doped with CuBr could reach a Bi-Sb alloy doped with CuBr could reach a power factor 3 times larger than that of a pure Bi-Sb alloy (Figure 7) [8]. It is suspected that the huge increase in power factor is a result of resonant levels.

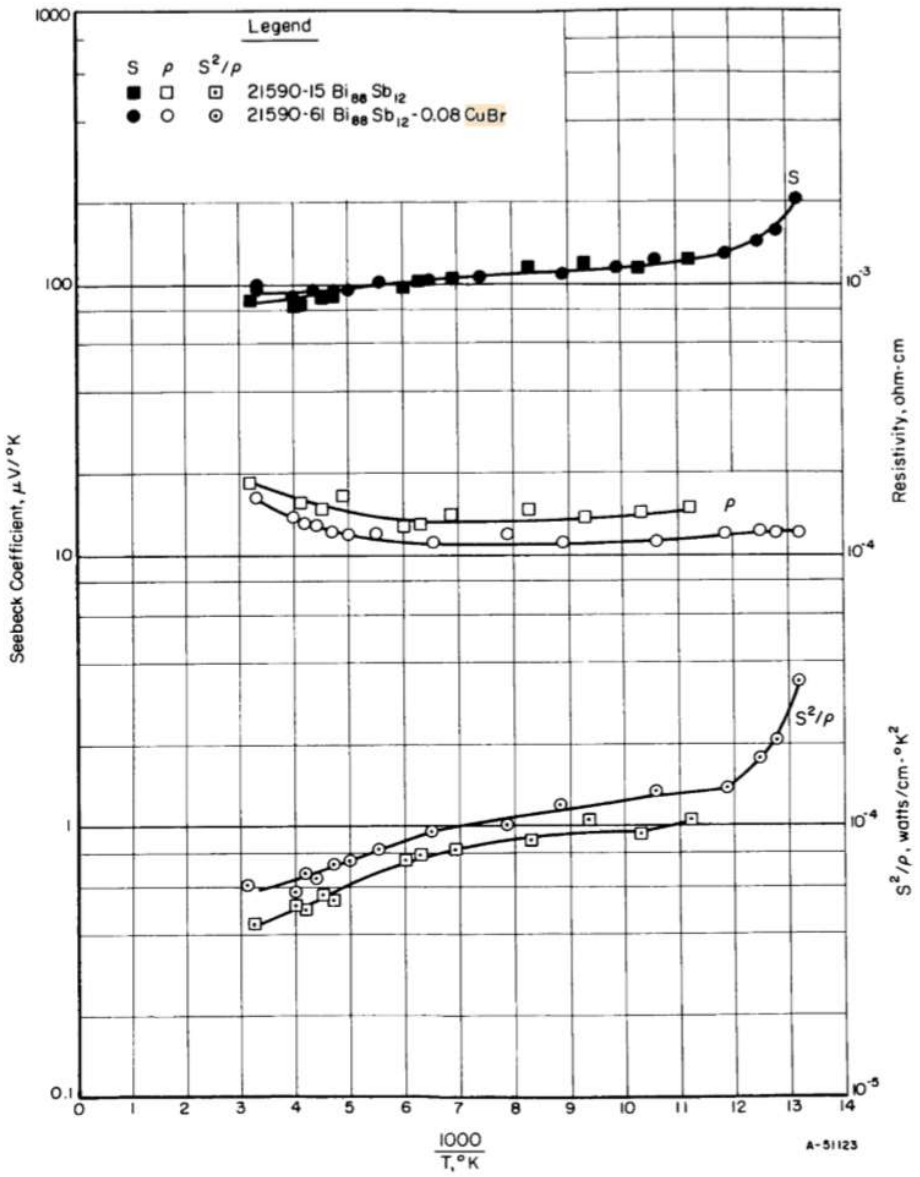

Figure 7: Seebeck Coefficient, Resistivity and S^2/ρ versus Reciprocal Temperature for n-Type (Doped and Undoped) $Bi_{88}Sb_{12}$ Alloys [8]

1.3 Overview of Thesis

This Thesis has 6 chapters, Chapter 2 discusses the experimental methods used. This including methods used to prepare polycrystalline and single-crystalline samples, sample structures used for measurement, and parameters that are measured. Chapter 3 discusses the measurement results of polycrystalline samples. This including results for mater sample with 0.5% CuBr, 2 times, 5 times and 10 times diluted 0.5% master samples, and master sample with 1% CuBr. Chapter 4 discusses the measurement results of single crystalline sample developed from 1% master sample. Chapter 5 discusses results of the entire project and future works that can further improve the results. Chapter 6, the conclusion, summarizes the key contribution of this thesis, discusses additional applications of this work.

Chapter 2: Experimental Methods

2.1 Sample Preparation

Polycrystals

A polycrystalline sample with high concentration of CuBr was prepared first. Stoichiometric amounts of pure Bismuth elements (5N) and pure Antimony elements (6N) were placed in an ampoule. The mole scale of Bismuth to Antimony is 88:12. The ampoule was then vacuumed and transported to glove box filled with Argon. 0.5 mole percent of CuBr powder was then added into the ampoule in the glove box, because CuBr is easily oxidized. The ampoule was then sealed under high vacuum, heated in a furnace under 700K for two days, and then water quenched. The master sample was then cut into pieces and placed in three empty ampoules, corresponding amount of pure Bismuth and Antimony elements were added into three ampoules to prepare 2 times, 5 times and 10 times diluted samples. All the ampoules were sealed under high vacuum, heated in a furnace under 700K for two days, and then water quenched.

Single Crystals

A single-crystalline sample was developed from the polycrystalline sample that has the highest zT, since it has been found that the best thermoelectric performance of Bi-Sb alloys can be obtained along the trigonal axis direction. The single-crystalline sample was developed using zone melting method. A hot coil moved along the ampoule with polycrystalline sample at a speed of 1mm/hour (Figure 8). The hot coil could melt the polycrystalline sample within a certain region. The molten zone moved with the hot coil, and single-crystalline sample was generated along path of the molten zone. Due to the fact that Bismuth and Antimony in the alloy have different melting points, further actions were taken to ensure the single-crystalline sample generated is in composition of $Bi_{88}Sb_{12}$.

Figure 8: Zone Melting Method

Phase diagram of Bi-Sb alloy is shown in Figure 9. Due to the difference in melting point, when liquid $Bi_{88}Sb_{12}$ starts to solidify at about 340K, the solid comes out will not be $Bi_{88}Sb_{12}$, instead the solid composition will be Antimony-rich. And composition of the liquid phase will move further left and become more Bismuth-rich. In that case, to obtain a $Bi_{88}Sb_{12}$ solid, the solidification must start from a liquid composition of $Bi_{97}Sb_3$. Moreover, in order to keep generating $Bi_{88}Sb_{12}$ solid, composition of the liquid phase has to be kept at $Bi_{97}Sb_3$, which means whatever amount of single-crystalline $Bi_{88}Sb_{12}$ is generated, the same amount of polycrystalline $Bi_{88}Sb_{12}$ needs to be added into the liquid phase.

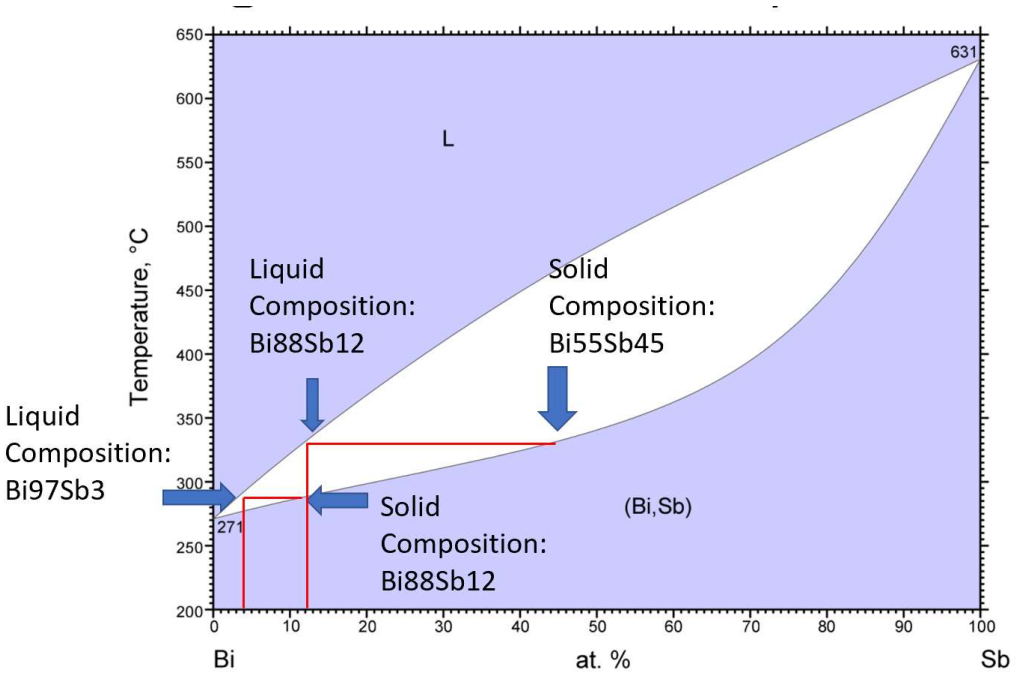

Figure 9: Phase Diagram of Bi-Sb Alloy [9]

In order to realize the situation mentioned above, a seed portion, with composition of $Bi_{97}Sb_3$ was placed in front of the $Bi_{88}Sb_{12}$ polycrystalline sample (Figure 10). The length of the seed portion is same as the length of molten created by hot coil. Thus, with the coil moving to the right, polycrystalline $Bi_{88}Sb_{12}$ was added into the molten zone when single-crystalline $Bi_{88}Sb_{12}$ was generated on the left. Moreover, to ensure same amount of $Bi_{88}Sb_{12}$ was solidified and liquified at the same time, the cross-section area of seed portion and feed portion have to be approximately the same. The ampoule was then sealed under vacuum, after which zone melting was conducted.

Figure 10: Seed and Feed portion before Zone Melting

2.2 Experimental Setup

For thermoelectric property measurement, the samples need to be cut into smaller sizes of approximately 1 to 1.5 mm length, 0.5 to 1 mm width, and 6.5 mm height. Before measurement, the specimen needs to be disposed first. A fragile and elaborate structure shown in Figure 11 was built.

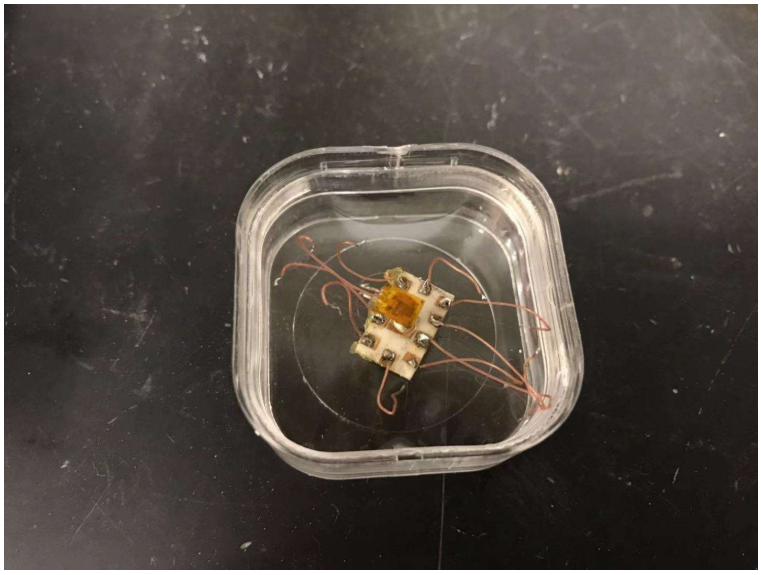

Figure 11: Sample Measurement Structure

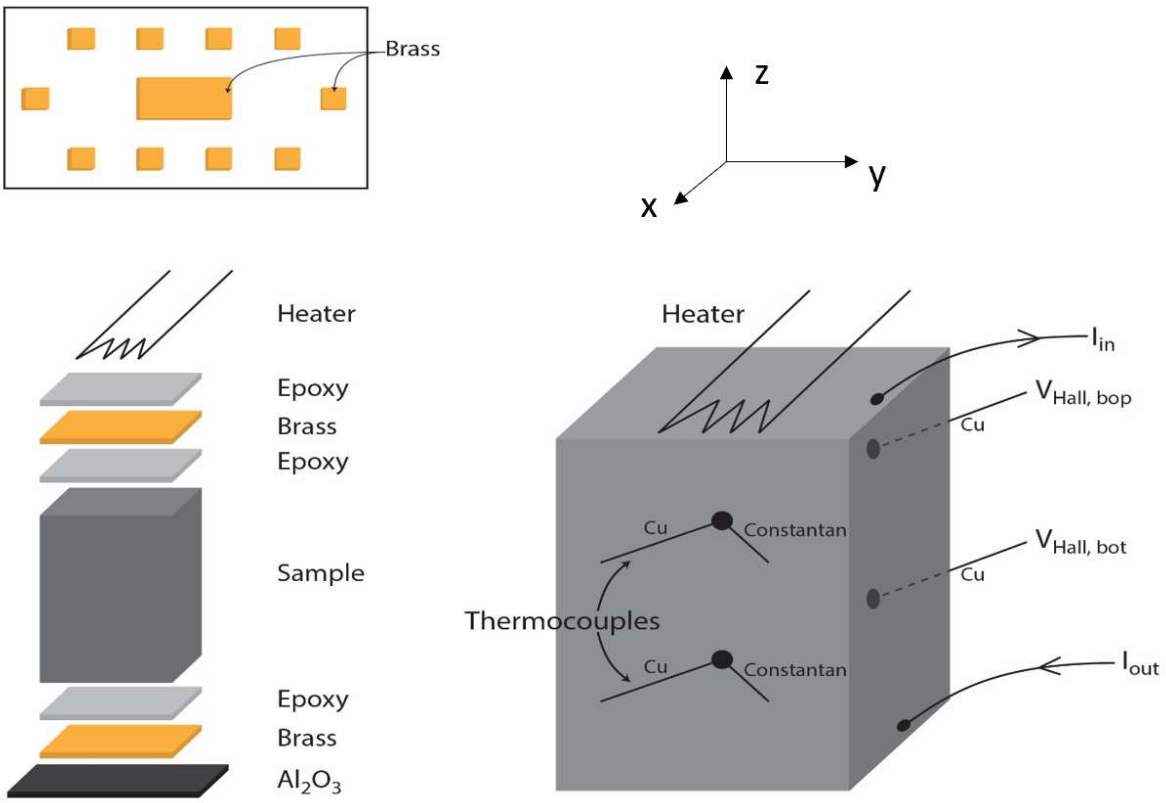

Figure 12: Schematic of Measurement Structure

A schematic of the structure is shown in Figure 12. A thin, Al_2O_3 plate 7.5 mm width and 12 mm length was used as the base for the structure. The reason Al_2O_3 was chosen here is because it is an excellent thermal conductor and can help drain out the heat so that the bottom of the sample can have a relatively lower temperature than the top of the sample. On the Al_2O_3 plate, 10 small chips of brass were glued with silver epoxy. In the center, a brass chip the same size as the bottom area of the sample also was glued with silver epoxy. Then, the sample was glued on the center brass chip with epoxy. On the top of the sample, another brass chip was glued. Then, a small heater was glued with silver epoxy on the brass chip to heat the upper part of the sample. The brass chips on the sample were used to distribute heat and current uniformly. As represented in the isometric view in Figure 12, there are 8 extremely thin wires attached to the sample, besides the heater mentioned above. These wires are spot welded on the sample.

Thin wires are used to minimize heat loss through the wires, but they are very fragile. To prevent them from breaking when connecting to the measurement device, they first are attached to the brass chips, which then are connected to the cryostat pin with normal wires (Figure 13). As shown in Figure 12, two copper-constantan thermocouples are spot welded on the front face of the sample. One is used to measure the hot side temperature, and the other is used to measure the cold side temperature. Two other copper wires are spot welded on the back surface to measure the hall voltage. The last two wires, connected to the top and bottom surface of the sample, respectively, provide a path for current to enter and leave the sample.

Figure 13: Cryostat used for measurement

After assembling the sample structure, it was attached to the measurement device to measure Seebeck coefficient, Hall voltage, thermal conductivity, and electric conductivity of the sample. Based on α, σ, κ, and T, the *ZT* value of the sample will be determined using Equation 1. To obtain parameters mentioned above, the z-direction is defined as parallel to the length of the sample, which is also the direction of current (I) passing through the sample. And the heat flux (q), current density (j_z), temperature gradient ($\nabla_z T$) and electric field (E_z) are defined as following:

$$q = \frac{Q_{in}}{A_c} = \frac{Q_{in}}{w \cdot th}, \tag{6}$$

$$j_z = \frac{I}{A_c} = \frac{I}{w \cdot th}, \tag{7}$$

$$\nabla_z T = \frac{T_{top} - T_{bot}}{z_{top} - z_{bot}} = \frac{T_{top} - T_{bot}}{L}, \tag{8}$$

$$E_z = \frac{\Delta V_z}{\Delta z} = \frac{V_{top} - V_{bot}}{z_{top} - z_{bot}} = \frac{V_{top} - V_{bot}}{L}, \tag{9}$$

where A_c is the cross-section area, w is the width, th is the thickness, and Q_{in} is heat provided by heater. With all the numbers given above, α, σ and κ can be calculated as following equations:

$$\alpha = \frac{\Delta V_z}{T_{top} - T_{bot}} + S_{copper} = \frac{V_{top} - V_{bot}}{T_{top} - T_{bot}} + S_{copper}, \tag{10}$$

$$\frac{1}{\sigma} = \rho = \frac{E_z}{j_z} = \frac{\Delta V_z \cdot w \cdot th}{I \cdot (z_{top} - z_{bot})} = \frac{\Delta V_z \cdot w \cdot th}{I \cdot L}, \tag{11}$$

$$\kappa = \frac{q}{\nabla_z T} = \frac{Q_{in} \cdot L}{(T_{top} - T_{bot}) \cdot w \cdot th}, \tag{12}$$

Hall measurements were also taken by passing a transverse magnetic field B along y-direction shown in Figure 12. The value of magnetic field swept from -1 to 1 Tesla for each data collecting point. Then, the Hall coefficient was calculated as follows:

$$R_H = \frac{E_x}{j_z B_y} = \frac{\Delta V_x \cdot w \cdot th}{I \cdot w \cdot B_y} = \frac{\Delta V_x \cdot th}{I \cdot B_y}, \tag{13}$$

and carrier concentration can be calculated from Hall coefficient with following equation:

$$n = \frac{1}{eR_H}, \tag{14}$$

Chapter 3: Characterization of Polycrystalline Bi-Sb alloys

3.1 Introduction

The reason why Bismuth (Bi) and Antimony (Sb) are interested as thermoelectric materials will be briefly discussed. As mentioned in chapter 1, Bi-Sb is regarded as a nontoxic and inexpensive substitution for PbTe alloys. Bismuth is a semimetal; whose valence band and conduction band have a small overlap. The overlap results in two types of charge carrier, which is not preferred. Because both types of charger carrier will move to the cold end, cancelling out the induced Seebeck voltages, and the Seebeck coefficient will become smaller. It is known that, by adding Sb into Bi, a band gap can be created and the Seebeck coefficient will increase. What's more, it has been confirmed that all of the Bi-Sb alloys between 3% and 16% antimony have a maximum z near $5 \times 10^{-3}/K$ at a temperature between 70K and 100K [10]. Furthermore, $Bi_{88}Sb_{12}$ was the alloy composition mentioned in the Battelle report [8]. So, an alloy composition of $Bi_{88}Sb_{12}$ was used in this project.

3.2 Master sample with 0.5% CuBr

Using method mentioned in chapter 2.1, a master sample with 0.5 mole percent CuBr was prepared first to check whether CuBr dopant can enhance power factor or not. Another pure $Bi_{88}Sb_{12}$ sample was prepared as reference sample. The 0.5% master sample and reference sample were then cut, mounted and measured. Results of Seebeck coefficient, electrical resistivity and thermal conductivity obtained are shown in Figure 14a, b& c.

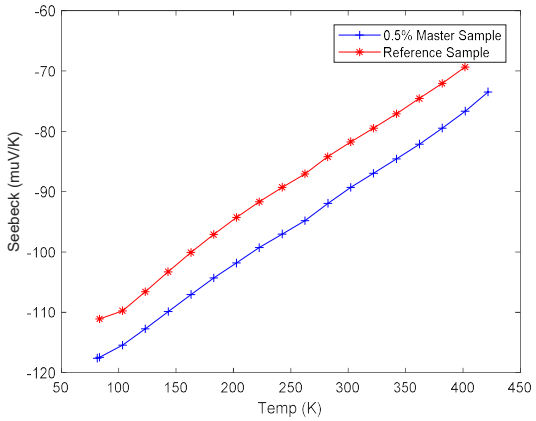

(a)

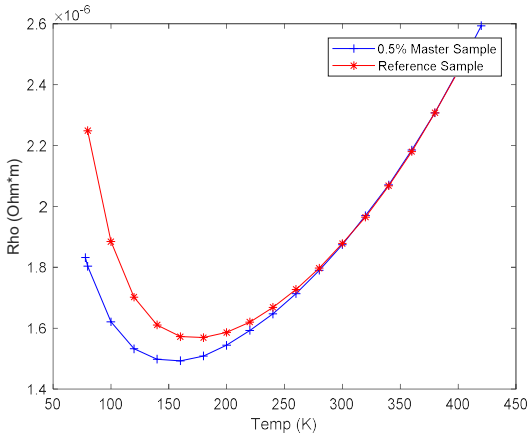

(b)

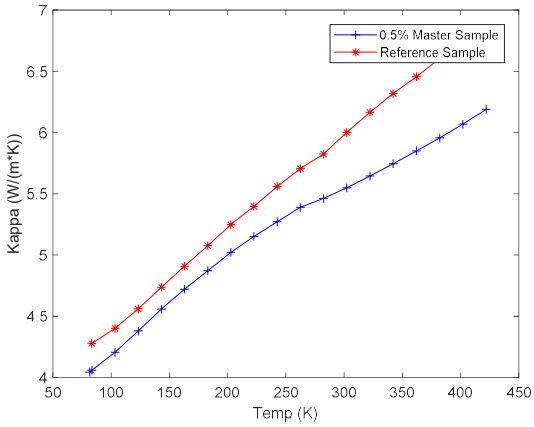

(c)

Figure 14 (a), (b) & (c): Seebeck Coefficient, Electrical Resistivity and Thermal Conductivity of $Bi_{88}Sb_{12}$ alloy with 0.5% CuBr dopant

As shown in Figure 14a, the 0.5% master sample has a higher Seebeck coefficient at all temperature points, which indicates that adding CuBr dopant does increase the thermopower of $Bi_{88}Sb_{12}$ alloy. The electrical resistivity was reduced slightly at low temperature (Figure 14b). The thermal conductivity was slightly reduced at all temperature (Figure 14c).

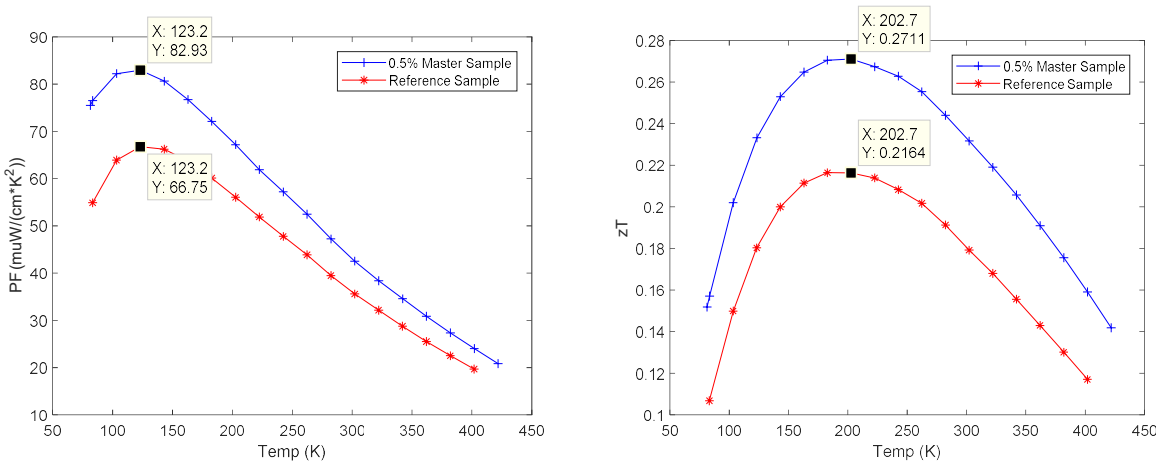

(a) (b)

Figure 15 (a) & (b): Power Factor and Figure of Merit of $Bi_{88}Sb_{12}$ alloy with 0.5% CuBr dopant with Maximum point labeled

As shown in Figure 15a, power factor of 0.5% master sample is larger than that of reference sample at any temperature point. The highest Seebeck coefficient value happened at 123.2K, where the power factor value was increased from 66.75 to 82.93 μW/(cm*K^2). As shown in Figure 15b, *zT* of 0.5% master sample is larger than that of reference sample at any temperature point. The highest *zT* value happened at 202.7K, where the *zT* value was increased from 0.216 to 0.271. The results are desired and confirm that CuBr dopant can enhance power factor of $Bi_{88}Sb_{12}$ alloy, However, whether 0.5% CuBr was the optimized amount was still unknown. To find out the optimized dopant amount, three diluted Samples derived from the 0.5% master sample were prepared.

3.3 Diluted Samples from 0.5% Master Sample

Using method mentioned in chapter 2.1, a set of diluted samples, 2 times, 3 times and 5 times diluted samples, were prepared to find the trend of power factor enhancement. All of three diluted samples were cut, mounted and measured. Results of Seebeck coefficient, electrical resistivity and thermal conductivity obtained are shown in Figure 16a, b& c.

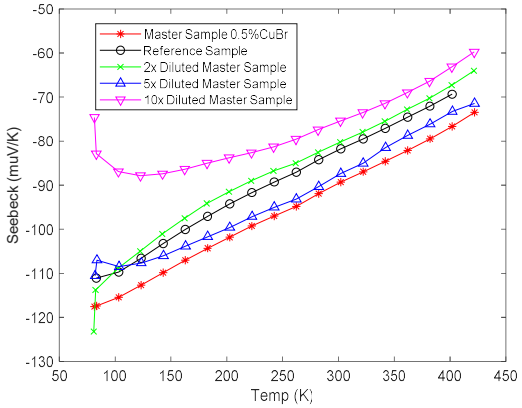

(a)

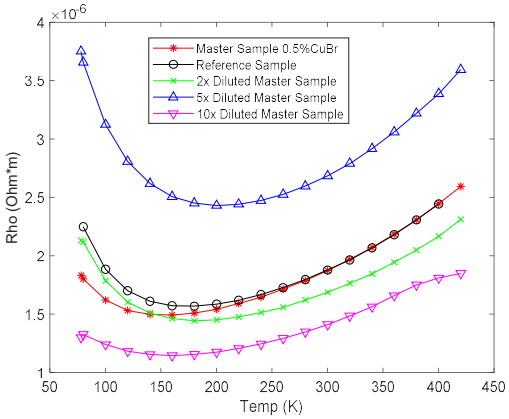

(b)

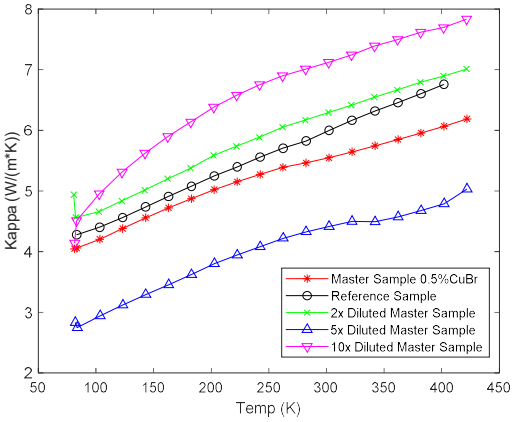

(c)

Figure 16 (a), (b) & (c): Seebeck Coefficient, Electrical Resistivity and Thermal Conductivity of Diluted 0.5% Master samples

As shown in Figure 16a, the 0.5% master sample has the highest Seebeck coefficient. The 10 times diluted sample has the lowest Seebeck coefficient. All the diluted samples have lower electrical resistivity values than reference sample dose, except the 5 times diluted sample which is much higher than other values (Figure 16b). All the diluted samples have higher thermal conductivity than reference sample dose, except the 5 times diluted sample which is much lower than other values (Figure 16c). The abnormal values of 5 times diluted sample's thermal conductivity and electrical resistivity are probably due to a crack within the sample.

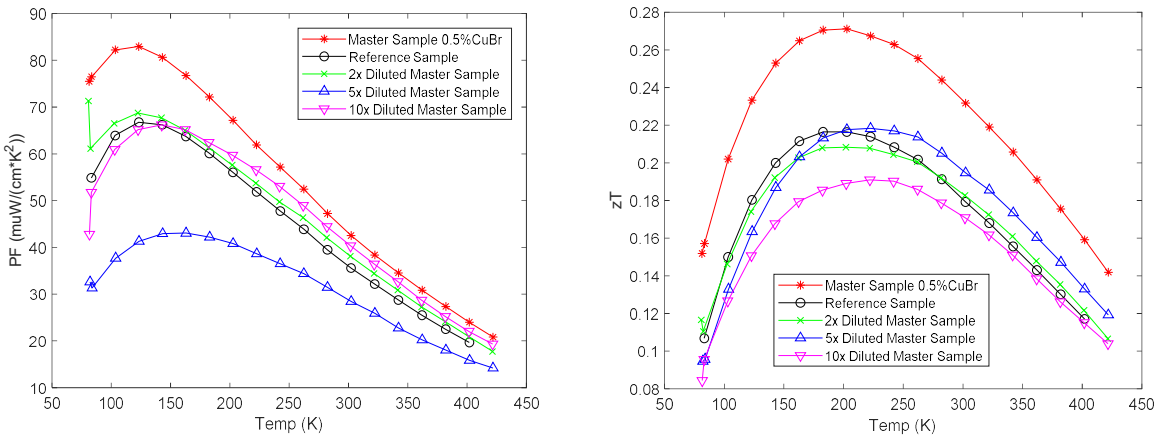

(a) (b)

Figure 17 (a) & (b): Power Factor and Figure of Merit of Diluted 0.5% Master Samples

Despite the erroneous power factor of 5 times diluted sample, other diluted samples have power factors similar to that of the reference sample, and the 0.5% master sample still has the highest power factor value (Figure 17a). For the value of *zT*, 0.5% master sample is still the highest, while *zT* values of diluted samples are very close to that of the reference sample (Figure 17b). Diluting dose not optimize neither power factor nor figure of merit. Master sample will higher dopant concentration should be prepared.

3.4 Master Sample with 1% CuBr

Using method mentioned in chapter 2.1, a master sample with 1 mole percent CuBr was prepared to check whether higher dopant concentration can further enhance power factor or not. The 1% master sample was cut, mounted and measured. Results of Seebeck coefficient, electrical resistivity and thermal conductivity obtained are shown in Figure 18a, b& c.

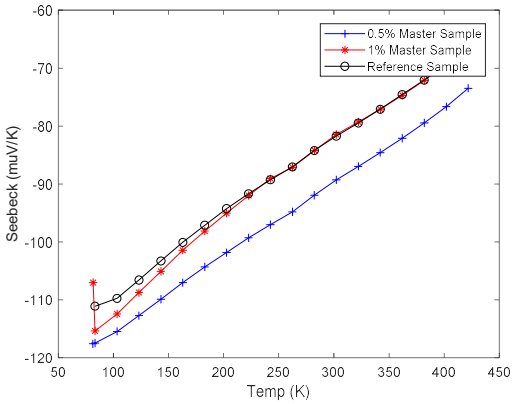

(a)

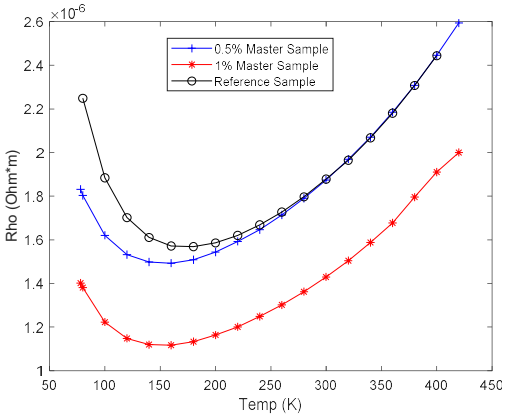

(b)

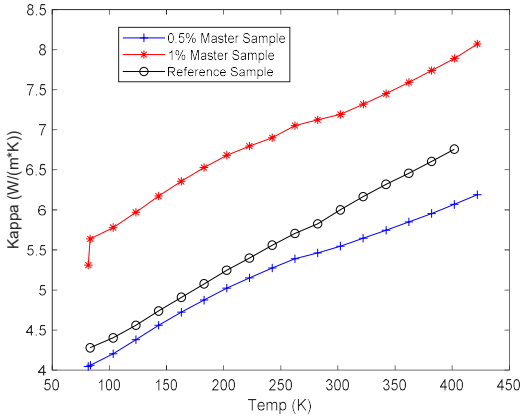

(c)

Figure 18 (a), (b) & (c): Seebeck Coefficient, Electrical Resistivity and Thermal Conductivity of $Bi_{88}Sb_{12}$ alloy with 1% CuBr dopant

As shown in Figure 18a, the 0.5% master sample still has a higher Seebeck coefficient at all temperature points. The 1% master sample has a high Seebeck coefficient only at low temperature. With the increase of temperature, Seebeck coefficient of the 1% master sample goes to that of the reference sample. However, the electrical resistivity of 1% master sample is much lower than that of reference sample and 0.5% master sample (Figure 18b). The thermal conductivity of 1% master sample also becomes much larger (Figure 18c).

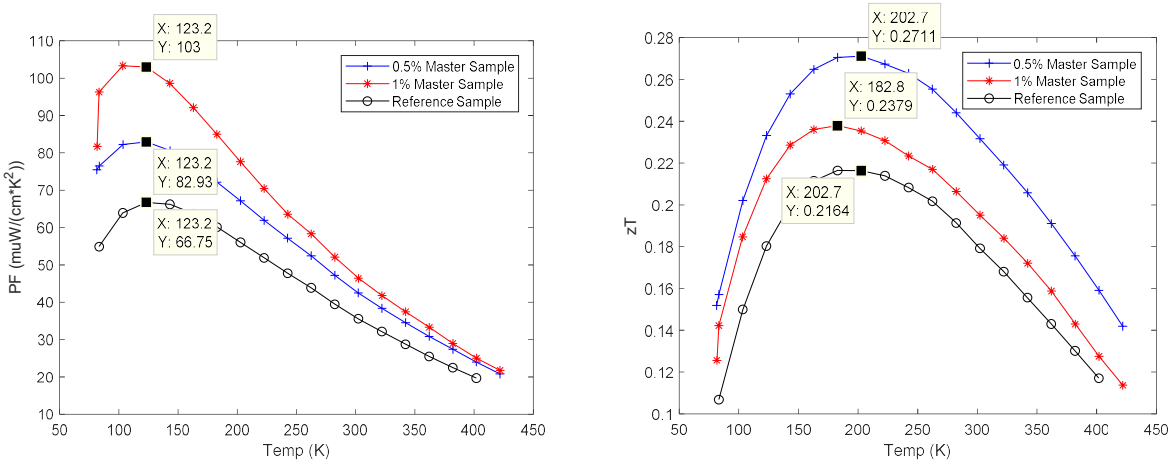

(a) (b)

Figure 19 (a) & (b): Power Factor and Figure of Merit of $Bi_{88}Sb_{12}$ alloy with 1% CuBr dopant with Maximum point labeled

As shown in Figure 19a, due to high Seebeck coefficient and low electrical resistivity, power factor of 1% master sample was greatly enhanced. The highest Seebeck coefficient value happened at 123.2K, where the power factor value was increased from 66.75 to 103 $\mu W/(cm*K^2)$. However, as shown in Figure 19b, *zT* of 0.5% master sample is still larger than that of 1% master sample at any temperature point. Because the thermal conductivity of 1% master sample is also increased. The highest *zT* value is still 0.271 from the 0.5% master sample. Although, the 0.5% master sample, has a higher *zT*, the 1% master sample has a much higher

power factor. Enhancement in power factor is the intended objective of resonant level. So, single-crystalline sample was generated using 1% master sample.

Chapter 4: Characterization of Single Crystalline Bi-Sb alloy

Using method mentioned in chapter 2.1, a single-crystalline sample with 1 mole percent CuBr was prepared to further improve the thermoelectric properties of $Bi_{88}Sb_{12}$ alloy. 1% master sample from chapter 3.4 was used as feed portion. A pure $Bi_{97}Sb_3$ was also prepared and used as seed portion. After zone melting, perfect single-crystalline sample was generated as shown in Figure 20. The single-crystalline sample was carefully cut with wire saw. And then, mounted and measured in trigonal direction, in which the thermopower is maximized. Results of Seebeck coefficient, electrical resistivity and thermal conductivity obtained are shown in Figure 21a, b& c.

Figure 20: Single-crystalline $Bi_{88}Sb_{12}$ alloy with 1% CuBr Dopant

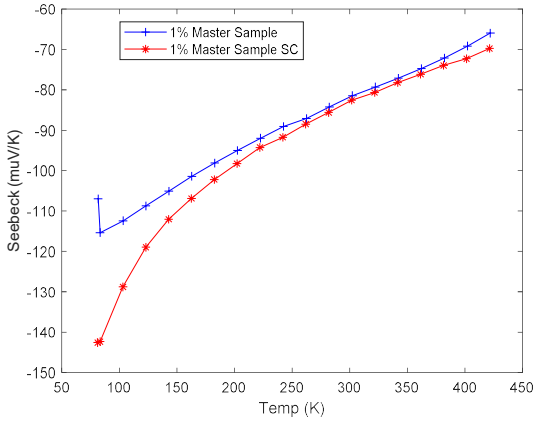

(a)

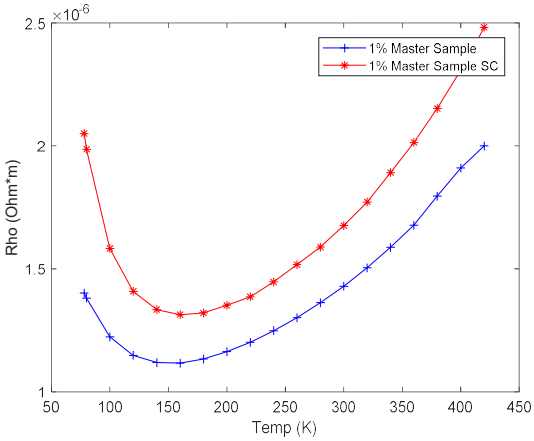

(b)

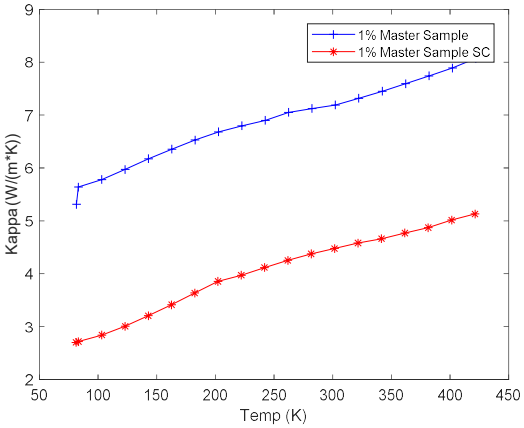

(c)

Figure 21 (a), (b) & (c): Seebeck Coefficient, Electrical Resistivity and Thermal Conductivity of Single-crystalline $Bi_{88}Sb_{12}$ alloy with 1% CuBr dopant

As shown in Figure 21a, Seebeck coefficient of single-crystalline sample was dramatically increased at low temperature, which is reasonable and desirable because single crystals were expected to have thermopower enhancement in trigonal direction. Also, the

electrical resistivity of single-crystalline sample was increased at all temperature points (Figure 21b). The thermal conductivity of single-crystalline sample was reduced at all temperature (Figure 21c). The changes for single-crystalline sample in electrical resistivity and thermal conductivity are also reasonable. Because in trigonal direction the thermal conductivity and electrical conductivity were both expected to decrease.

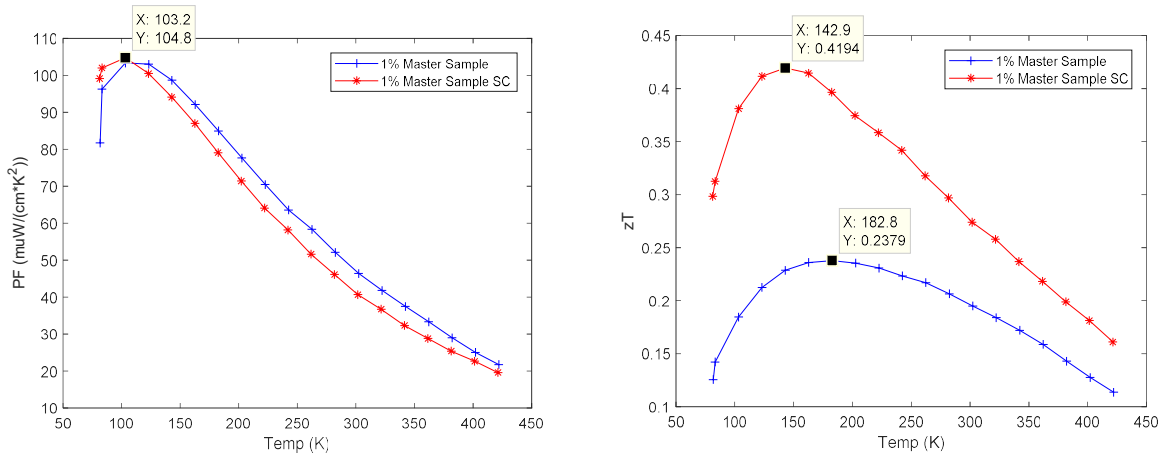

(a) (b)

Figure 22 (a) & (b): Power Factor and Figure of Merit of Single-crystalline $Bi_{88}Sb_{12}$ alloy with 1% CuBr dopant with Maximum point labeled

Although the Seebeck coefficient of single-crystalline sample was increased at low temperature, the electrical resistivity was also increased. So single-crystalline sample's power factor is almost the same as that of the polycrystalline sample. As shown in Figure 22a, no enhancement in power factor was observed. The highest power factor value is 104.8 μW/(cm*K^2). The *zT* value of single-crystalline sample was enhanced greatly, because the thermal conductivity was reduced (Figure 22b). The highest *zT* value happened at 142.9K, where the *zT* value was increased to 0.419, which almost doubled the *zT* value of reference sample. The results are desired and confirm that CuBr dopant can enhance power factor of $Bi_{88}Sb_{12}$ alloy, and single-crystallization can further enhance the *zT* value. However, the performance of Bi-Sb alloy can still be improved.

Chapter 5: Discussion

5.1 Source of Error

There are many sources of error introduced in this experiment. One error is from the measurement of chemicals used in samples. The amount of chemicals used in each sample is documented in Appendix A. The error of this part is within 1%, which is not the major contribution. Another error is from the ingot casting procedure. It is very likely that CuBr power does not distribute uniformly in the alloy and the solubility of CuBr in Bi-Sb alloy is still unknown. In that case it's hard to determine the actual amount of CuBr within the measured sample piece. To check the composition of measured samples, XRF (X-Ray Fluorescence) is needed. For single-crystalline sample, the zone melting method also introduced some error. Because of the inherent purification function of zone melting method, the dopant concentration in single-crystalline sample may not be the same as the 1 % master sample. Again, XRF is needed to check actual amount of dopant.

5.2 Results discussion

As mentioned in chapter 3 & 4, data collected shows that 0.5% master sample has enhancement in Seebeck coefficient, power factor and zT value. While diluted samples show no obvious enhancement in either of the thermoelectric properties. The 1% master sample, however, has greater enhancement than 0.5% master sample dose, due to the small electrical resistivity 1% master sample has. However, the zT value of 1% master sample is smaller than that of 0.5% master sample, because of the high thermal conductivity 1% master sample has. For single-crystalline sample, the Seebeck coefficient was increased a lot at low temperature in trigonal

direction. However, electrical conductivity and thermal conductivity were both decreased in trigonal direction. As a result, the power factor of single-crystalline sample was not increased and the *zT* value was increased a lot.

Generally, desired results were obtained through this experiment. Obvious enhancement in power factor was observed by adding CuBr dopant into $Bi_{88}Sb_{12}$ alloy. Further enhancements of thermopower and *zT* were also observed in trigonal direction of the single-crystalline sample. But the result is not as good as reported by Battelle, and there is still room for improvement. Comparing the results of Battelle to the results obtained in this experiment, a major difference can be found. At low temperature, the electrical resistivity in Battelle tends to be flat. Yet, in all of the electrical resistivity plots mentioned above, the electrical resistivity tends to increase at a steep slope. This could result in relatively smaller enhancement in power factor shown in this experiment. To further improve the power factor, electrical resistivity has to be reduced at low temperature.

5.3 Next Step

To find out the reason of increasing electrical resistivity at low temperature, the result of $Bi_{88}Sb_{12}$ was compared to that of pure bismuth (Figure 23). Different from the trend of $Bi_{88}Sb_{12}$ alloy's electrical resistivity, pure bismuth's electrical resistivity tends to decrease with temperature. It is desirable to have a low electrical resistivity, because a low electrical resistivity at low temperature will lead to a much larger power factor. Reducing the amount of antimony in the alloy might be way to achieve the goal mentioned above.

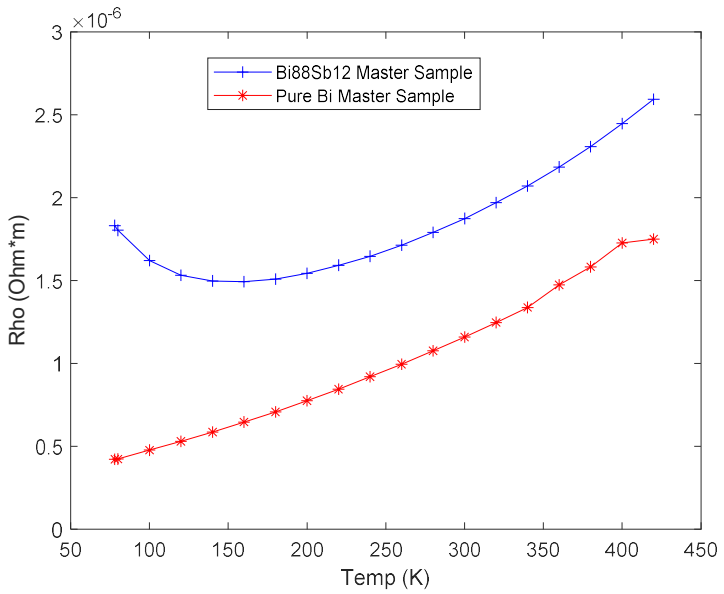

Figure 23: Electrical Resistivity of Pure Bismuth Master Sample.

The same trend of electrical resistivity was also confirmed by Smith and Wolfe. As shown in Figure 24, $Bi_{95}Sb_5$ has an electrical resistivity decreasing with temperature. Also, as mentioned in their paper, Seebeck coefficient of both $Bi_{88}Sb_{12}$ and $Bi_{95}Sb_5$ are close to -110 μV/K at around 100K (Figure 25). So, it is reasonable to measure a sample of $Bi_{95}Sb_5$ with 1% CuBr dopant for next step. Also various amount of CuBr dopant can be added to optimize the power factor.

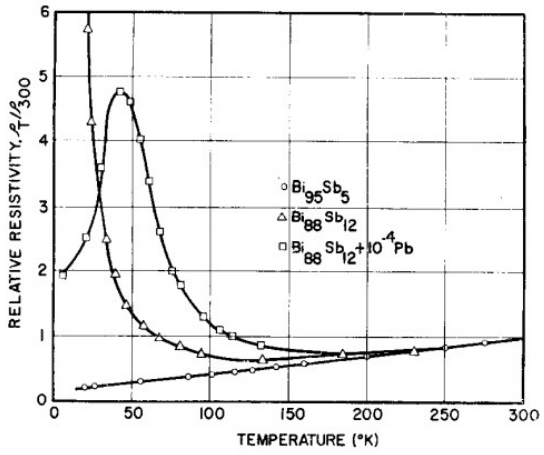

Figure 24: Variation of electrical resistivity of Bi-Sb Alloys [10]

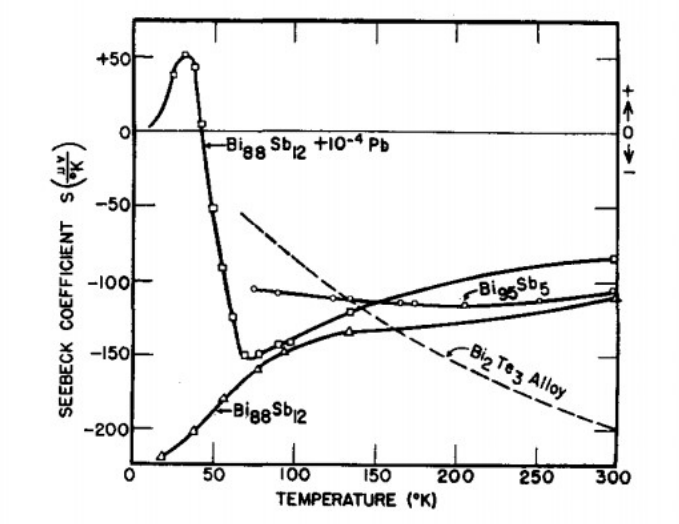

Figure 25: Variation of Seebeck coefficient of Bi-Sb Alloys [10]

Chapter 6: Conclusion

The purpose of this project is to increase the total efficiency of thermoelectric coolers by improving the performance of thermoelectrical materials. The results of this project show that the main purpose has been accomplished.

6.1 Contributions

Thermoelectric coolers are devices working based on thermoelectrical effect. Comparing to traditional compressor-based cooler, thermoelectric cooler has advantages in every aspect except lower efficiency. To increase the efficiency of thermoelectric cooler, efforts have been devoted into the improvement of thermoelectric materials' performance. However recent improvement of thermoelectric materials' performance was done with PbTe alloy. The excellent thermoelectric properties of PbTe alloy are preferred. However, the high price of tellurium and the restricted use of lead makes impractical for wide use.

Bi-Sb alloys, which are nontoxic and relatively cheaper, make good substitutions for PbTe alloy. Although pure Bi-Sb alloy have moderate thermoelectric properties, adding CuBr dopant to the alloy was confirmed to enhance the thermoelectric properties hugely. The CuBr doped Bi-Sb alloy has the potential to be widely used in the future.

6.2 Additional Applications

The idea of resonant dopant can not only be used on Bi-Sb alloys. It is also suitable for other materials. Resonant doping method provides an possibility to increase the value of zT by

increasing the power factor, which is different from normal ways a decreasing lattice thermal conductivity. What's more, the improvement of thermoelectric materials' performance will not only benefit thermoelectric coolers but also thermoelectric generators used for transforming waste heat into electricity.

6.3 Summary

Several Bi-Sb alloys with different amount of CuBr dopant was prepared and measured in this project. After measurement, CuBr dopant was confirmed to enhance the power factor of Bi-Sb alloy. Perfect single crystals were developed with zone melting method. Further enhancements of thermopower and zT were observed in single-crystalline samples. However, the enhancement was not as large as previously reported. To further increase the thermoelectric properties, a CuBr doped Bi-Sb alloy with less Sb amount will be measured in the future.

Reference

[1] Xiao, Chong. "*Synthesis and Optimization of Chalcogenides Quantum Dots Thermoelectric Materials"* (2016).

[2] Snyder, G. J., & Toberer, E. S. "*Complex thermoelectric materials*". *Nature Materials*, *7*(2), 105-114 (2008).

[3] "*How Does a Thermoelectric Cooler (TEC) Work*?" *Thermalbook.wordpress.com*, thermalbook.wordpress.com/how-does-a-thermoelectric-cooler-tec-work/ (2018).

[4] Zlatić, Veljko, and A C. Hewson. *Properties and Applications of Thermoelectric Materials: The Search for New Materials for Thermoelectric Devices*. Dordrecht: Springer (2009)

[5] Brown, D. R., N. Fernandez; J. A. Dirks, T. B. Stout. *"The Prospects of Alternatives to Vapor Compression Technology for Space Cooling and Food Refrigeration Applications"*. Pacific Northwest National Laboratory (PNL). U.S. Department of Energy (2010).

[6] Heremans, Joseph P, Vladimir Jovovic, Eric S. Toberer, Ali Saramat, Ken Kurosaki, Anek Charoenphakdee, Shinsuke Yamanaka, and G J. Snyder. *"Enhancement of Thermoelectric Efficiency in Pbte by Distortion of the Electronic Density of States." Science*. 321.5888 (2008).

[7] Biswas, K, J He, M.G Kanatzidis, I.D Blum, D.N Seidman, V.P Dravid, C.-I Wu, and T.P Hogan. *"High-performance Bulk Thermoelectrics with All-Scale Hierarchical Architectures." Nature*. 489.7416 (2012).

[8] E. P. Stambaugh, L. K. Matson, B. G. Koehl, R. Simon, and E. H. Lougher. *"Development of improved Thermoelectric Materials for Spacecraft Applications."* Battelle Memorial Institute. (1964).

[9] *ASM Alloy Phase Diagrams Center*. ASM International. apdredirect.asminternational.org (2007).

[10] G.E. Smith, and R. Wolfe. *"Thermoelectric Properties of Bismuth-Antimony Alloys."* *Journal of Applied Physics*. 10.1063 (1962).